CHEMISTRY
A European Journal

A Journal of
ChemPubSoc Europe

Accepted Article

Title: Exploring the Relationship between BODIPY Structure and Spectroscopic Properties to Design Fluorophores for Bioimaging

Authors: Joanna L Donnelly, Daniel Offenbartl-Stiegert, José M Marín-Beloqui, Loris Rizello, Guiseppe Battaglia, Tracey M Clarke, Stefan Howorka, and Jonathan David Wilden

To be cited as: *Chem. Eur. J.* 10.1002/chem.201904164

Link to VoR: http://dx.doi.org/10.1002/chem.201904164

Supported by
ACES

WILEY-VCH

10.1002/chem.201904164

WILEY-VCH

FULL PAPER

Exploring the Relationship between BODIPY Structure and Spectroscopic Properties to Design Fluorophores for Bioimaging

Joanna L. Donnelly, Daniel Offenbartl-Stiegert, José M. Marín-Beloqui, Loris Rizello, Guiseppe Battaglia, Tracey M. Clarke, Stefan Howorka*, and Jonathan D. Wilden*

Abstract: Designing chromophores for biological applications requires a fundamental understanding of how the chemical structure chromophore influences its photophysical properties. We here describe the synthesis of a library of BODIPY dyes, exploring diversity at various positions around the BODIPY core. The results show that the nature and position of substituents have a dramatic effect on the spectroscopic properties. Substituting in a heavy atom or adjusting the size and orientation of a conjugated system provides a means of altering the spectroscopic profiles with high precision. The insight from the structure-activity relationship was applied to devise a new BODIPY dye with rationally designed photochemical properties including absorption towards the near-infra red. The dye also exhibited switch-on fluorescence to enable visualization of cells with high signal-to-noise ratio without washing-out of unbound dye. The BODIPY-based probe is non-cytotoxic and compatible with staining procedures including cell fixation and immunofluorescence microscopy.

Joanna L. Donnelly, Daniel Offenbartl-Stiegert, Dr. José M. Marín-Beloqui, Dr. Loris Rizzello, Prof Guiseppe Battaglia, Dr. Tracey M. Clarke, Prof. Stefan Howorka and Dr. Jonathan D. Wilden
Department of Chemistry, University College London
20 Gordon Street, London, WC1H 0AJ (UK)
E-mail: j.wilden@ucl.ac.uk; s.howorka@ucl.ac.uk

Joanna L. Donnelly, Daniel Offenbartl-Stiegert, Prof. Stefan Howorka and Dr. Jonathan D. Wilden, Institute of Structural and Molecular Biology, University College London
20 Gordon Street, London, WC1H 0AJ (UK)

Dr. Loris Rizzello and Prof. Guiseppe Battaglia
Institute of Physics of Living System, University College London
Gower Street, London, WC1E 6BT

Dr. Loris Rizzello and Prof. Guiseppe Battaglia
IBEC-Institute for Bioengineering of Catalonia, The Barcelona Institute of Science and Technology, 08028 Barcelona, Spain

Prof. Guiseppe Battaglia
ICREA-Institució Catalana de Recerca i Estudis Avançats, 08010 Barcelona, Spain

Introduction

The use of fluorophores for cellular imaging is vital for diagnostics, biological discovery, and biomedical research. Visualising cells with small-molecule probes is of particular interest as, unlike quantum dots or fluorescent proteins, can be designed to permeate cell membranes.[1,2] The development of chromophores with suitable optical properties is key. Tailoring dyes to meet bioimaging demands requires, however, a fundamental understanding of the relationship between chromophore structure and the spectroscopic properties.[3,4] Understanding the structure-property relationship can, for example, help generate structures capable of absorbing in the far-red (FR) and near infra-red (NIR) regions of the electromagnetic spectrum.[5,6] Such molecules would eliminate the need to use shorter wavelength light that can be toxic to cells. NIR light can also reach deeper into biological tissue to expand the observational horizon. While many FR and NIR fluorophores with excellent optical properties exist, they are often unsuitable for *in vivo* applications due to various issues including hydrophobicity, aggregation, and non-specific binding to a multitude of cellular targets.[5,7]

Boron dipyrromethene (BODIPY) dyes are ideal to explore the relationship between structure and spectroscopic properties given their popular use in cellular imaging. BODIPY dyes combine desirable chemical, physical and spectroscopic properties[7–11] including chemical stability, absorption maxima (λ_{max}) around or above 500 nm, sharp fluorescence emission, and good quantum yields for the resulting fluorescence.[5,6,12–15] Sharp excitation and emission peaks enable precise detection by confocal fluorescence microscopy. The small aromatic and rigid BOPIDY core has both a high extinction coefficient and strong fluorescence emission[16] present a good template to synthesize a range of analogues with longer absorption wavelengths.[6,9–11] Reflecting these advantages, BODIPY dyes have been employed as molecular probes for bio-imaging, molecular detection, photocaging, photodynamic therapy, and as antimicrobials and laser dyes.[17–20]

However, for fluorophores containing the BODIPY core, absorption intensity is often compromised in analogues where absorbance λ_{max} has been shifted towards the far-red region. Similarly, a compromise between fluorescence λ_{max} and intensity is often observed.[5,7] Previous work has focused on the synthetic challenge of generating BODIPY analogues and the independent evaluation of each individual compound's optical, chemical and

10.1002/chem.201904164

physical properties.[5,7,10,11,21] In general, previous attempts to define systematic and predictive information regarding particular substituents or substitution sites[22] have, therefore, focused on the type of modification made to the BODIPY skeleton and rationalising the changes in absorbance and fluorescence *via* computational and orbital treatments of the data involved.[7,11,13,23]

Here, we take an alternative approach by preparing a library of analogues with substitutions at various positions on the BODIPY skeleton to sample a large chemical space. Using this information, we have generated a correlation table, describing the effect that various substitution patterns have. This relationship between chemical structure and spectroscopic properties allowed us to develop the basic understanding of synthetic modifications to the BODIPY core which can be used to rationally guide future efforts. Following the data presented in the table, we have successfully designed and synthesised a novel BODIPY fluorophore (HiBO) to obtain the optimal spectroscopic characteristics. HiBO was explicitly designed as a cell staining dye with specific attributes: (i) molecular selectivity towards the targeted biological structure. (ii) A "light switch" effect[24,25] whereby the fluorescence signal increases upon binding to a target. This achieves minimal background signal obviating the requirement for washing steps to remove residual unbound probe. (iii) Long emission wavelength in the optical window above 700 nm to allow deep-tissue imaging and maximize signal-to-noise thereby exploiting the low endogenous cellular fluorescence in this spectroscopic region. (iv) Biocompatibility in terms of minimal cytotoxicity. Finally, (v) ease-of-use and adaptability to most standard staining procedures including live cell imaging, fixation, and immunofluorescence microscopy to broaden the application range.

Results and Discussion

We began by preparing a small library of analogues with various substituents at different positions around the BODIPY nucleus to sample a large chemical space.

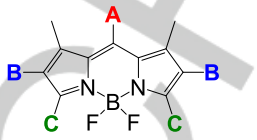

Figure 1. BODIPY scaffold showing the sites of modification in this study. (**A**) *meso,* (**B**) 2,6 and (**C**) 3,5.

Modifications were carried out at the *meso* (**A**), 2,6 (**B**) and 3,5 (**C**) positions of the BODIPY nucleus. Modifications selected were predominantly small molecular changes, with the aim that this would facilitate highly specific fine-tuning of properties with excellent precision. The molecules prepared are outlined in Figure 2. The photophysical properties of each analogue were measured in both polar and non-polar media. The results are outlined in Table 1 and SI Figure S1.

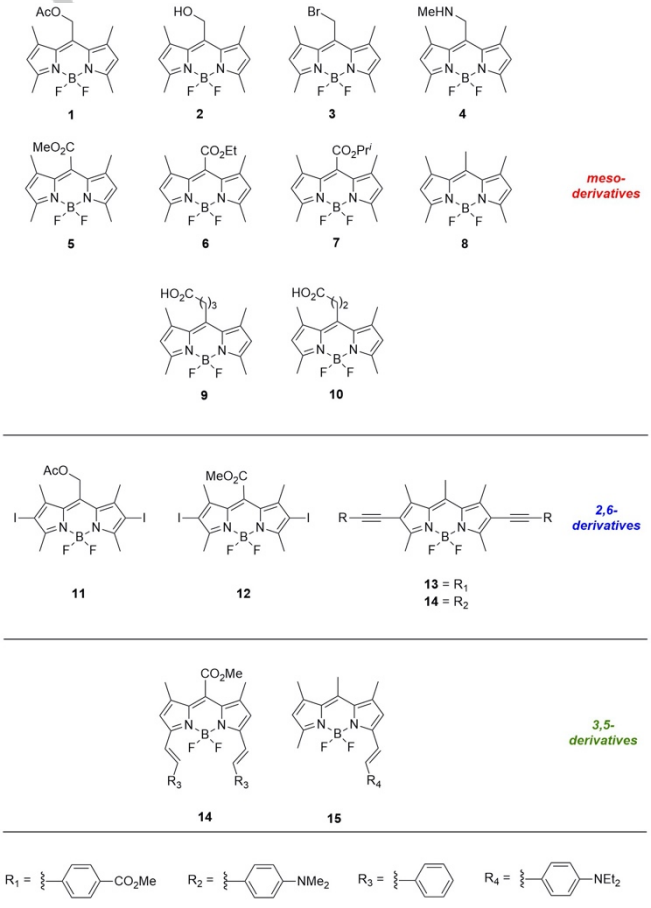

Figure 2. Structures of the BODIPY analogues synthesized.

10.1002/chem.201904164

Table 1. Summary of photophysical data for compounds **1-16**. For fluorescence measurements the compounds were excited at $\lambda_{max, abs}$.

Compound	Solvent	$\lambda_{max, abs}$ (nm)	ε ($M^{-1}cm^{-1}$)	$\lambda_{em, fluor.}$ (nm)
1	DMSO	504	8,250	569
	Hexane	511	3,250	558
2	DMSO	509	225,370	522
	Pet. ether	505	99,470	517
3	DMSO	525	5,010	523
	Hexane	530	9,570	516
4	DMSO	509	18,030	531
	MeCN	505	19,890	528
5	DMSO	509	5,000	526
	Hexane	511	3,250	527
6	DMSO	509	33,340	537
	Pet. ether	511	37,850	541
7	DMSO	512	39,790	537
	Pet. ether	511	47,270	534
8	DMSO	509	132,610	507
	Pet. ether	511	649,010	501
9	DMSO	499	5,650	514
	MeCN	495	5,230	511
10	DMSO	499	1,550	n/a
	MeCN	496	1,620	520
11	DMSO	554	17,540	591
	Pet. ether	555	2,190	571
12	DMSO	555	17,550	590
	Pet. ether	549	31,280	576
13	DMSO	535	2,420	583
	DCM	547	43,640	589
14	MeCN	559	980	528
	DCM	590	21,280	n/a
15	DMSO	657	8,910	672
	Pet. ether	642	14,440	658
16	DMSO	704	14,980	738
	Pet. ether	679	3,740	696

We first chose to explore the effect of different substitutions on the *meso*-position (Figure 1, A, compounds 1-10) as this site is readily functionalised *via* a variety of straightforward synthetic approaches. A range of substituents were chosen based on steric bulk, polarity and ease of preparation. Furthermore, substitutions that are reported extensively in the literature, such as *meso*-aryl substitutions, were left out.[26,27] This led to a total of ten examples of diversity at this site. In general, we observed that the larger bulky groups, such as ester or carboxylic acids group (compounds 1, 5-7, 9-10), facilitated a bathochromic shift in the absorbance maximum. However, the absorption extinction coefficient (ε) was compromised in comparison to unsubstituted compound 8. At present, it is unclear why such a dramatic difference in ε is observed. However, given that there is no difference in the conjugation of the BODIPY core framework between compound 8 and compounds 9 and 10, it seems likely that the difference results from intermolecular aggregation or other supramolecular interactions (e.g. H-bonding, π-stacking, and electrostatic effects) between individual molecules rather than any change in the electronic properties of the individual molecules. Another possibility is that the introduction of substituents that possess n-type orbitals, for example the oxygen atom in carbonyls, possibly give rise to new n-π* transitions. These tend to be lower in energy than π- π*, and are always weaker.

We then proceeded to explore functionalisation at the 2- and 6-positions (Figure 1, B, compounds 11-14). The symmetrical nature of the BODIPY molecule often allows both 2- and 6-positions to be substituted, thereby magnifying the resultant spectral changes. The inclusion of heavy iodine atoms at the 2 and 6-positions (compounds 11 and 12) resulted in a significant absorbance λ_{max} red-shift of up to 50 nm compared to the corresponding compounds 5 and 1. As an added benefit, iodine also provides a gateway to incorporation of more complex conjugated systems with the potential for more extensive modification of the compounds spectroscopic properties. Appending an alkyne bearing a methylbenzoate moiety (i.e. adding extended conjugation to these sites, compounds 13 and 14) also leads to a longer absorbance wavelength of up to 40-50 nm compared to compound 8; however, the extinction coefficient and fluorescence intensity are both compromised compared to the unsubstituted example, compound 8. The increase in λ_{max} is desirable for *in vivo* applications, but other key spectral properties are compromised, making such compounds less desirable for imaging and other biological applications.

Furthermore, we proceeded to explore the effect of substitution at the 3- and 5-positions of the BODIPY core (Figure 1, C, compounds 15 and 16). It has been noted that these are relatively reliable for selective modification due to the significant proton acidity difference between positions 3 and 5, and positions 1 and 7.[11] This was achieved by functionalisation *via* base-catalysed Knoevenagel condensation with aromatic aldehydes. In both cases a dramatic and desirable absorbance λ_{max} displacement towards the infrared was observed. This effect was found to be more substantial for compound 16. Despite being only

10.1002/chem.201904164

monosubstituted, this analogue contains a diethylamino group as an auxochrome. When compared to their reference compounds 5 and 8, the solvatochromic shift between the two solvents is also almost twice as large with the monosubstituted compound 16 than with the double substituted compound 15. This is due to the introduction of the diethylamino group only present in compound 16.[28,29]

Finally, bandgaps for all compounds were computationally calculated using time dependant density functional theory (TD-DFT) calculations. For the calculations of compounds 11 and 12, iodine was substituted by bromine as iodine is not compatible with this calculation base. The TD-DFT calculations (CAM-B3LYP/6-31g*, SI Figure S2 and Table S1) determined the ground state geometries and relative molecular orbital (HOMO and LUMO) energies with their corresponding band gaps for each of the BODIPY analogues. The computationally predicted results correlate well with the experimental data (Table 1, SI Figures S1 and S2 as well as SI Table S1).

After carefully examining the spectral properties of these compounds both experimentally and computationally, we proceeded to systematically correlate the effects of substitution with different functional groups. This, we envisaged, would allow the construction of designer molecules with specific spectral properties based on reference to our previous findings. The results of the above discussion are condensed in Table 2.

Table 2. Summary of substitution effects on the spectral properties of BODIPY. The arrows signify an increase or decrease. A double arrow denotes a stronger change.

Position	Modification	λ_{max} (nm)	ε ($M^{-1}cm^{-1}$)	λ_{em} (nm)	Solvatochro-mism
A	Me and OH groups	-	↑	↑	-
	Long alkyl chains	↓	-	-	-
	Bulky groups	-	↓	↓	-
	Carbonyl/ amine groups	-	-	↓	-
B	Extended conjugation	↑	↓	↑	↑
	Heavy atoms	↑	↑	-	-
	Auxo-chromes	↑	-	↓	↑
C	Extended conjugation	↑↑	↑	↑	↑
	Auxo-chromes	↑	↑	↑	↑

The nature and positioning of substituents clearly has a strong effect on the resultant spectroscopic properties. The results indicate that the most efficacious methods to fine-tune these properties are *via* the 3 and 5 positions of the BODIPY core. Combined with other modifications throughout the structure, these molecules can therefore afford a broad spectrum of chromophores for highly specialised applications.

Having established this framework for predicting the spectral properties of substituted BODIPY compounds, we decided to test the reliability of our predictions by designing a new compound. The new fluorophore, termed HiBO, was rationally designed as an environmentally sensitive membrane dye (Figure 3).

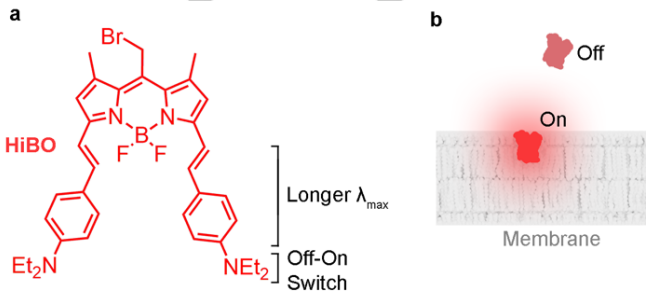

Figure 3. Principle mechanism of environmentally-sensitive membrane fluorophore HiBO, its structure and synthesis. a) Near infra-red fluorophore HiBO highlighting the principles that guided its rational design. b) Schematic representation of the environmentally dependent activation of the fluorophore upon insertion into a lipid bilayer.

To attain an absorption wavelength closer to the IR, two benzene-based moieties were added to the BODIPY core. The substituents were placed at positions 3 and 5, which are known from the previous results (compounds 15 and 16) to accommodate substitutions that result in a more red-shifted absorption wavelength (Figure 3).[5] Furthermore, to induce strong solvatochromism, which is essential for environmental sensing, two diethyl-amino groups were installed (Figure 3).[28,29] Amino groups can render fluorophores highly sensitive to solvent polarity[30] and also contribute to longer absorption wavelengths.[29] The compact amphiphilic design of HiBO is aimed to counter common issues of other long wavelength, yet lipophilic non-BODIPY probes, such as poor biological compatibility, compromised fluorescence emission and limited retention within membranes.[31] Finally, the selection of bromine on the *meso*-position should allow for bioconjugation of the dye in follow-up studies. HiBO was prepared by standard techniques (see experimental section) and its absorption characteristics were measured in both polar and non-polar solvents. The results are outlined in Table 3 and SI Figures S3 and S4.

Table 3. Summary of UV-Vis absorption properties of HiBO.

Solvent	λ_{max} (nm)	ε ($M^{-1}cm^{-1}$)
DMSO	734	16,130
Pet. ether	699	17,880

Spectroscopic analysis determined the degree to which the chemical modifications increase absorption wavelengths and

10.1002/chem.201904164

result in the desired solvent-dependency. The UV-Vis absorption spectrum of HiBO acquired in polar solvent DMSO displayed a maximum wavelength of 734 nm. The extinction coefficient of HiBO at this wavelength, 16,130 $M^{-1}cm^{-1}$ (Table 3), is similar to other BODIPY scaffolds and higher than the alternative: substituted porphyrin dyes.[32] By contrast, more apolar solvents revealed a strong environmental dependency in the absorption characteristics. For example, in petroleum ether, absorption was 699 nm reflecting a shift of 35 nm relative to a polar environment (Table 3 and SI Figure S3 and S4). This solvatochromism is in-line with the rational design and can be attributed to the two diethyl-amino moieties.[27] The observations also match predictions from TD-DFT calculations which were used to model the orbitals of HiBO in solvents of different polarity (ether, acetonitrile and methanol) and calculate the energy gaps of the different electronic transitions (SI Figures S5-S7).

Furthermore, testing in a variety of organic solvents revealed that differences in polarity showed a strong influence on fluorescence emission intensity and maximum wavelength (SI Figure S4 and Table S2). Specifically, fluorescence quantum yield measurements showed that fluorescence emission intensity increases from apolar to polar solvents by a factor of up to 16 (SI Table S2). The decrease in the quantum yield along with a decrease in solvent polarity was also consistent with a change in the Stokes shift observed in different solvents (SI Figure S8). The Stokes shift for HiBO was 0.05 eV in ether and 0.15 eV in methanol and acetonitrile. This indicates that relaxation prior to photoluminescence in apolar solvents, i.e. ether, requires negligible deformation of the geometry compared to polar solvents. This lack of geometry deformation implies little displacement of the potential energy surface of the S_1 excited state compared to the ground state, increasing the overlap between the involved orbitals, and therefore increasing the radiative relaxation pathway. This significant environmental dependence validates the experimental design and supports sensitive fluorescence imaging of cells. Furthermore, the correlation table can be used to design novel fluorophores with the desired polarity and fluorescence response.

For follow-on membrane bindings studies, HiBO was dissolved in DMSO at a concentration of 10 mM and diluted into PBS buffer to final concentrations ranging from 6 to 50 µM.

The cell staining properties of HiBO were initially tested using synthetic giant unilamellar vesicles (GUVs) formed from 1-palmitoyl-2-oleoyl-sn-glycero-3-phosphocholine (POPC) lipids. Incubation of HiBO with GUVs resulted in effective staining within 5 min, as shown by confocal fluorescence microscopy (SI Figure S9). The notable short period of time required for imaging was achieved without washing to remove excess dye. Prior to applying HiBO for cell staining, the non-toxicity of the dye was confirmed. In viability studies, hypopharyngeal squamous carcinoma cells (FaDu)[34] were treated with up to 50 µM fluorophore for up to 24 h. This concentration is five times higher than what was used for staining. In the MTT assay readout, cell viability was not significantly impacted even at the highest concentration of HiBO and the longest time period (SI Figure S10). We are therefore confident that HiBO is not cytotoxic

The HiBO fluorophore was applied to visualize biological cells. FaDu cells were incubated for 30 min with HiBO at a concentration of 10 µM. Staining resulted in strong fluorescence labelling of the cellular membranes and cytoplasm observed *via* confocal fluorescence microscopy (Figure 4a; the HiBO-stained cells are shown in red). Complementary staining for 5 and 60 min established an increase in fluorescence intensity with incubation duration (Figure 4c, SI Figure S11).

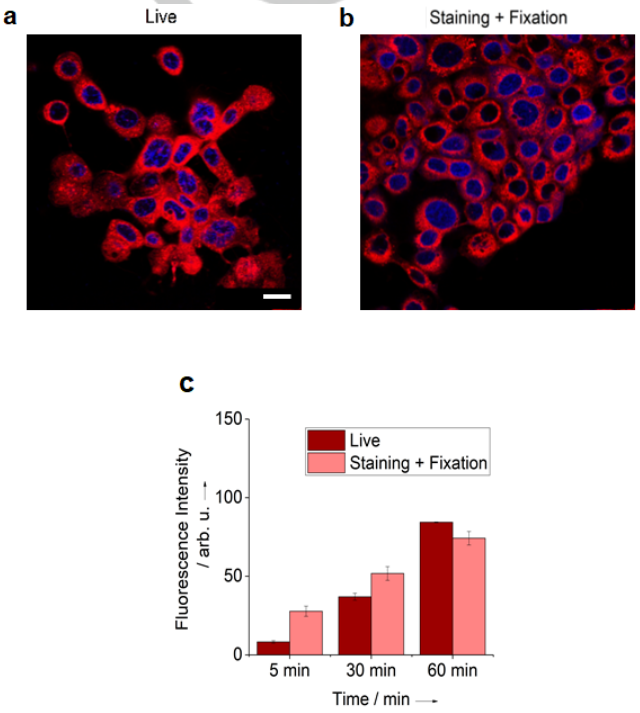

Figure 4. Confocal microscopy images of FaDu cells incubated with HiBO and DAPI nuclear stain. Visualisation was carried out using lasers emitting at 633 nm (red) and 405 nm (blue). a) Live cells incubated with HiBO for 30 min. b) Cells fixed with paraformaldehyde after incubation with HiBO for 30 min. c) Effect of incubation time on fluorescence intensity in live and fixed cells. All incubations carried out using 10 µM solution of HiBO in PBS buffer. The data represent averages and standard deviations from four repeats. The fluorescence microscopy slice images were taken using the same exposure, and no fluorescence adjustments were made to images. Scale bars are 25 µm for all images. Single channel images in SI Figures S11, S12 and S13.

To further explore staining, cells were treated with HiBO for 30 min followed by fixation with paraformaldehyde (Figure 4b, SI Figure S13). The intensity observed for live cells increased with incubation time to 60 min from approximately 8 arb.u. to over 80 arb.u. more than 10-fold (Figure 4c). The intensity for fixed cells more than doubled from 27 to over 70 (arbitrary units). The fluorescence intensity at 5 and 30 min was more intense than for stained live cells, which could be a result of molecular retention of

the fluorophore within the cross-linked membrane. Staining after fixation also allowed visualization of the cytoplasmic membrane and intracellular compartments, yet less intensely than with post-fixation (SI Figures S12 and S13). Likely, the cross-linked bilayer structure reduced the dyes accessibility. The data suggest that the fluorescent probe is suitable for sensitive staining of cells in both live cells and with fixation.

We next investigated whether sensitive labelling using HiBO was compatible with membrane permeabilisation, which is required for immunofluorescence microscopy. Cells were incubated with HiBO for 1 h, then treated with 0.1 % of detergent (Triton X), followed by monitoring fluorescence emission over time. After 10 min, the cytoplasmic membranes were still clearly visible despite a small decrease in fluorescence emission (Figure 5a, SI Figure S15). This high degree of resistance to permeabilization is unusual for membrane dyes which are normally not retained in the lipid bilayer during lipid perturbation.

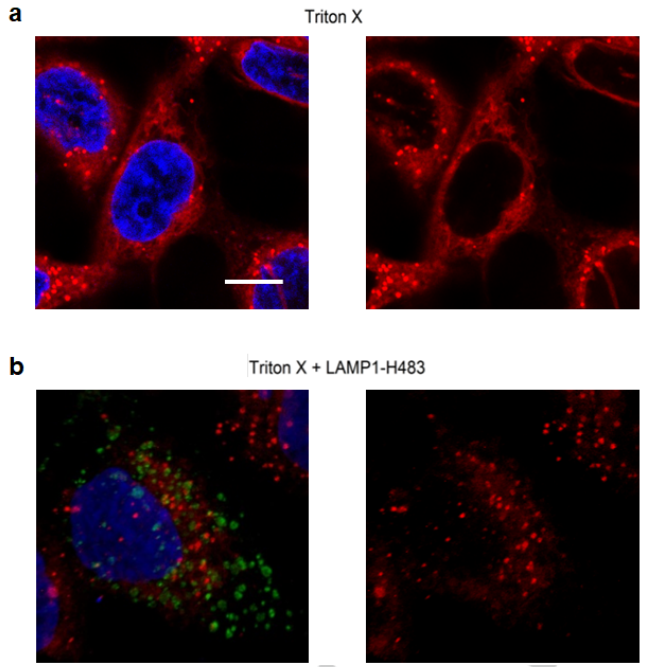

Figure 5. Confocal microscopy images of FaDu cells to demonstrate compatibility of HiBO-membrane staining with permeabilisation, DNA DAPI, and protein antibody labelling. a) Cells were fixed with para-formaldehyde, incubated 60 min with HiBO and treated with 0.1% Triton X. The images show left the DAPI (blue) and HiBO (red) channel, and right HiBO. b) Cells were fixed with paraformaldehyde, HiBO-stained, permeabilised, BSA-blocked and labelled with LAMP1-H483 and Donkey A488 anti-rabbit antibodies. The image on the left shows DAPI (blue), A488 (green) and HiBO (red) channels. The image on the right only displays HiBO. The fluorescence was adjusted to indicate presence of HiBO in the membrane. Scale bars 10 µm.

After establishing compatibility with permeabilization, HiBO was used in conjunction with immunofluorescence (IF) microscopy. Cells were first incubated with HiBO followed by a typical IF protocol (i.e. fixation with paraformaldehyde, permeabilization with Triton X, and blocking with BSA to minimize non-specific binding of antibodies). For IF, antibody LAMP1-H483 against lysosomal membranes was used along with a secondary antibody labelled with fluorophore Alexa488. The resultant images display the antibody clearly labelling the target lysosomes (Figure 5b, SI Figure S16, green channel). The stain remained clear (Figure 5b, SI Figure S16, red channel) suggesting that HiBO is highly compatible with IF microscopy.

Conclusions

We have prepared a library of BODIPY analogues with systematic variation at defined points around the molecule's core. Measurement and analysis of the spectral properties has allowed us to correlate specific substitutions and functional groups to spectral properties. This has allowed us to draw up a correlation table which can be used to rationally design molecules with particular desirable characteristics. We have exemplified our approach by the preparation of a smart switchable near-infrared fluorophore (HiBO) for the specific and sensitive imaging of cells. HiBO stains both synthetic membranes and cells with excellent signal-to-noise ratio without the need to remove excess dye. The fluorophore tolerates both fixation and permeabilization and is appropriate for use in combination with other imaging methods such as antibody staining with minimal interference. Furthermore, the imaging of lipid bilayers does not compromise cell viability. The dependence of emission wavelength and intensity on different hydrophobic environments will potentially help to probe bilayers of different composition. Similarly, the long wavelength of HiBO is orthologous to other fluorophores and expected to permit multicolour imaging to track multiple cellular components or processes. The combined desirable properties of HiBO will help visualise lipid bilayers in cells, tissues and organisms to promote research and diagnostics.

Experimental Section

Chemicals and solvents: All solvents and reagents were obtained from Sigma Aldrich, Acros Organics, Alfa Aesar or Thermo Fischer Scientific. All materials were used as received unless otherwise stated.

Chromatography: Monitoring of all reactions was achieved using 60 F254 silica coated aluminium TLC plates by Merck. Visualisation of these was carried out using light of wavelength of 254 and/or 365 nm. Purification was achieved by flash column chromatography using silica gel (43 – 60 µm) from Merck.

Spectroscopic analysis: ^{1}H, ^{13}C and ^{11}B nuclear magnetic resonance spectra were recorded at 600 MHz using the Bruker Avance III 600 Cryo or the Avance Neo 700 as specified. Chemical shifts are reported in ppm relative to internal standard TMS as follows: chemical shift, multiplicity (s = singlet, d = doublet, t = triplet, q = quartet, sep = septet, m = multiplet),

coupling constant(s), integration and assignment using either $CDCl_3$ or DMSO-d6 as a solvent and TMS as an internal standard. UV-vis spectra were obtained with the Cary 100 UV/Vis spectrophotometer between 800-200 nm. Fluorescence spectra were acquired using the Agilent Cary Eclipse Fluorescence Spectrophotometer with emission measured between 1000-200 nm. UV-vis and fluorescence spectra were analyzed using the Agilent Cary WinFLR software.

Fluorescence quantum yield: PLQY was measured with a Horiba FluoroMax-4 spectrofluorometer with an integrating sphere and corrected for instrument response at the exciting wavelength. A HiBO concentration of 10 µM in MeCN, Et_2O and MeOH in a 1 mm length cuvette was used for these experiments.

LCMS and HRMS measurements: All reverse phase UPLC-MS measurements were carried out using an Acquity Ultra Performance LC Waters system equipped with a UPLC BEH C18 column (50 x 2.1 mm, 1,7 mm beads). Gradient conditions were run using two mobile phases; mobile phase A: 0.1% formic acid in water; mobile phase B: 95% acetonitrile-5% water. Sample injections of 1 µL were used. Flow from the column immediately entered a mass spectrometer, the Waters SQ Detector, which was configured with an electrospray ionisation source with nitrogen used as the nebuliser gas. Mass spectra were obtained by scanning at a speed of 10,000 Da/sec up to 2,000 Da. The Waters MassLynx Mass Spectrometry Software was used for data acquisition post analysis. All EI and CI mass spectrometry was carried out using the Thermo Finnigan MAT900 magnetic sector. ESI was carried out using the Waters Autosampler Manager 2777C with Waters LCT Premier Q-TOF. Where relevant, ammonia was used as the reagent gas prior to analysis. Please note that it was difficult to obtain good quality data in LCMS or HRMS for some of the compounds. We believe this is due to degradation upon ionisation.

Preparation of giant unilamellar vesicles (GUV)[35]: GUVs were prepared by electroformation using Nanion Vesicle Prep Pro equipment. Two aliquots of POPC (6 µL, 25.4 mM in $CHCl_3$) were deposited on an indium tin oxide glass plate inside two rubber rings and the solvent left to evaporate. The rings were flooded with sucrose (600 µL, 1 M in water) and another indium tin oxide glass plate placed on top. The protocol for the electroformation involved a 3 min rise time to a frequency of 10 Hz and an amplitude of 3 mV in a sinusoidal fashion which was held for 120 min. After a fall time of 5 min, GUVs were obtained and found to have a diameter between 1-30 µm.

Cell culture of mammalian cells: Pharynx squamous carcinoma cell lines (FaDu) were obtained from American Type Culture Collection (ATCC HTB-43) FaDu were grown in DMEM containing 10% fetal bovine serum (FBS), supplemented with 2 mM L-glutamine, 1 mM sodium pyruvate, 100 U/mL penicillin and 100 µg/mL streptomycin. Cells were sub-cultured, or seeded for further analyses, by incubation with trypsin-EDTA solution (Sigma-Merck). Cell fixation was carried out by incubation of 3.7% of paraformaldehyde (in PBS) for 7 min, followed by extensive washing in PBS.

MTT cell viability assay: Cell viability was evaluated using an MTT (3-(4,5-Dimethylthiazol-2-yl)-2,5-diphenyltetrazolium bromide) based assay. Briefly, 8 × 104 cells/well were seeded overnight on 96 well-plates, and then incubated with HiBO at final concentrations of 0, 6, 12.5 and 50 µM. Each batch was incubated for 1, 3, 6 and 24 h in eight different duplicates. The plates were scanned on a well-plate spectrophotometer at 570 nm. Data have been normalized to the control (untreated cells), and a t-test was used for statistical analyses

Confocal microscopy[35]: Microscopic analyses were carried out using the Leica SPEinv (inverted SPE) microscope (vesicles) or the Leica TCS SP8 (cells), using single photon irradiation with sequential scanning. With this set up, filters are not needed. Instead, one manually sets the Hybrid Detectors to the wavelength needed for a specific dye Moreover, in order to avoid absolutely any possible signal overlap, the instrument works in sequential mode, where each single fluorophore undergoes an excitation and emission cycle independently. The machine switches on and off each channel (both laser and detectors) to avoid fluorescence overlap. The objective used for cell images was a 63X immersion oil with NA of 1.4. Visualization of giant unilamellar vesicles was carried out in a buffer of 0.5% TAE, 500 mM NaCl. Visualization of cells was carried out in PBS. Images were taken using excitation wavelengths of 532 or 635 nm using cells on fluorodish cell culture dishes from World Precision Instruments. Data were analysed using LAS-X (Leica Application Suite X) software.

Synthetic procedures

Compound 1: A solution of dry DCM (30 mL) was degassed before 2,4-dimethylpyrrole (0.22 mL, 2.1 mmol, 2 eq.) was added followed by acetoxyacetyl chloride (0.14 mL, 1.3 mmol, 1.2 eq.). The reaction mixture was heated under reflux for two hours under argon after which it was cooled to room temperature. DIPEA (0.73 mL, 4.2 mmol, 4 eq.) was added dropwise prior to stirring for 15 minutes. $BF_3{\cdot}Et_2O$ (0.53 mL, 4.2 mmol, 4 eq.) was added and the reaction mixture was stirred for 30 minutes under argon and protected from the light. The solvent was removed *in vacuo* to yield a dark red solid which was purified by flash column chromatography on silica gel; eluent: hexane/DCM:30/70 to afford (5,5-difluoro-1,3,7,9-tetramethyl-5*H*-4λ^4,5λ^4-dipyrrolo[1,2-*c*:2',1'-*f*][1,3,2]diazaborinin-10-yl)methyl acetate (182 mg, 0.57 mmol, 53%) as a red solid. ^{1}H-NMR (600 MHz, $CDCl_3$) δ_H 6.09 (s, 2H, C**H**), 5.30 (s, 2H, C**H$_2$**), 2.54 (s, 6H, 2C**H$_3$**), 2.36 (s, 6H, 2C**H$_3$**), 2.14 (s, 3H, C**H$_3$**) ppm; ^{13}C NMR (151 MHz, $CDCl_3$) δ_C 170.7, 156.8, 141.6, 133.4, 122.4, 115.5, 58.0, 20.7, 15.8, 14.8 ppm; ^{11}B-NMR (224 MHz, $CDCl_3$) δ_B 0.56 (t, *J* = 33.3 Hz) ppm; ^{19}F-NMR (658 MHz, $CDCl_3$) δ_F -146.4 (q, *J* = 32.5 Hz) ppm; IR (C=O) = 1738.72 cm^{-1}; Rf (hexane/DCM:20/80) = 0.5.

Compound 2: A solution of (5,5-difluoro-1,3,7,9-tetramethyl-5*H*-4λ^4,5λ^4-dipyrrolo[1,2-*c*:2',1'-*f*][1,3,2]diazaborinin-10-yl) methyl acetate (255 mg, 0.80 mmol, 1eq.) in THF (8.0 mL) was flushed with argon. LiOH (95 mg, 4.0 mmol, 5 eq.) was dissolved in distilled water (8.0 mL) and the two solutions were combined and stirred at room temperature under argon and protected from the light for four hours. The organic material was extracted using EtOAc and the organic layers were washed with brine (3 x 20 mL) and saturated NH_4Cl (1 x 20 mL) before being dried over $MgSO_4$, filtered under vacuum and the solvent removed *in vacuo*. The crude red solid was purified by flash column chromatography on silica gel; eluent: hexane/DCM:10/90. The fractions containing product were combined and concentrated under vacuum to yield (5,5-difluoro-1,3,7,9-tetramethyl-5*H*-4λ^4,5λ^4-dipyrrolo[1,2-*c*:2',1'*f*][1,3,2]diazaborinin-10-yl)methanol (172 mg, 0.62 mmol, 78%) as a red solid. ^{1}H NMR (600 MHz, *d*^{6}-DMSO) δ_H 6.24 (s, 2H, 2C**H**), 5.56 (t, *J* = 5.2 Hz, O**H**), 4.71 (d, *J* = 5.2 Hz, 2H, C**H$_2$**), 2.49 (s, 6H, 2C**H$_3$**), 2.41 (s, 6H, 2C**H$_3$**) ppm; ^{11}B-NMR (224 MHz, $CDCl_3$) δ_B -1.62 ppm; ^{19}F-NMR (658 MHz, $CDCl_3$) δ_F -146.5 (q, *J* = 32.2 Hz) ppm; IR (O-H) = 3548.59 cm^{-1}; R_f (hexane/DCM:20/80) = 0.1.

Compound 3[36]**:** Dry DCM (150 mL) was evacuated with argon. Bromoacetyl bromide (0.170 mL, 1.90 mmol, 1 eq.) and 2,4-dimethylpyrrole (0.400 mL, 3.90 mmol, 2 eq.) were added dropwise and the dark red reaction mixture was stirred at room temperature under argon and protected from the light for three hours. The solvent was reduced to ~50 mL under vacuum and TEA (4.00 mL, 29.0 mmol, 15 eq.) was added. After 15 minutes of stirring under argon, $BF_3{\cdot}Et_2O$ (8.00 mL, 65.0 mmol, 33 eq.) was added dropwise. The reaction mixture was stirred for a further three hours under argon and protected from the light. DCM was used to extract the organic material which was washed with distilled water, dried over $MgSO_4$, filtered and concentrated *in vacuo*. The crude red product was purified by flash column chromatography on silica gel; eluent: hexane/DCM from a ratio of 80/20 to 50/50. The fractions containing product were combined and concentrated by evaporation to afford 10-(bromomethyl)-5,5-difluoro-1,3,7,9-tetramethyl-5*H*-4λ^4,5λ^4-dipyrrolo[1,2-*c*:2',1'-*f*][1,3,2]diazaborinine (224 mg, 0.660 mmol, 35%) as a red solid. ^{1}H-NMR (600 MHz, $CDCl_3$) δ_H 6.09 (s, 2H, C**H**), 4.69 (s, 2H, C**H$_2$**Br), 2.54 (s, 12H, 4C**H$_3$**) ppm; ^{13}C-NMR (151 MHz, $CDCl_3$) δ_C 156.6, 141.0, 137.3, 131.1, 122.4, 24.7, 16.1, 14.8 ppm; ^{11}B-NMR (224 MHz, $CDCl_3$) δ_B 0.62 (t, *J* = 32.5 Hz) ppm; ^{19}F-NMR (658 MHz, $CDCl_3$) δ_F -146.7 (q, *J* = 33.1 Hz) ppm MS (EI) $C_{14}H_{16}BBrF_2N_2$ (*m/z* 340.1, [M{^{79}Br}+H]$^+$; *m/z* 342.1, [M{^{81}Br}+H]$^+$; *m/z* 261.1, [M-Br+H]$^+$); R_f (hexane/DCM:50/50) = 0.4

Compound 4: 10-(bromomethyl)-5,5-difluoro-1,3,7,9-tetramethyl-5*H*-4λ^4,5λ^4-dipyrrolo[1,2-*c*:2',1'-*f*][1,3,2]diazaborinine (70 mg, 0.20 mmol), KI (58 mg, 0.348 mmol, 1.7 eq.) and K_2CO_3 (160 mg, 1.10 mmol, 5.8 eq.) were dissolved in dry THF (15 mL) and flushed with argon. The reaction mixture was stirred overnight. The solvent was removed *in vacuo* and the crude purified by flash column chromatography on silica gel; eluent: hexane/EtOAc:10/90. The fractions containing product were combined and concentrated to afford 1-(5,5-difluoro-1,3,7,9-tetramethyl-5*H*-4λ^4,5λ^4-dipyrrolo[1,2-*c*:2',1'-*f*][1,3,2]diazaborinin-10-yl)-*N*-methylmethanamine as a purple solid (34.0 mg, 0.117 mmol, 57%). ^{1}H NMR (600.130 MHz, $CDCl_3$) δ_H 6.07 (s, 2H, 2C**H**), 3.90 (s, 2H, C**H$_2$**), 2.56 (s, 3H, C**H$_3$**), 2.52, (s, 6H, 2C**H$_3$**), 2.47 (s, 6H, 2C**H$_3$**) ppm; ^{11}B-NMR (224 MHz, $CDCl_3$) δ_B 0.56 (t, *J* = 33.3 Hz) ppm; ^{19}F-NMR (658 MHz, $CDCl_3$) δ_F -146.6 (q, *J* = 32.5 Hz) ppm; IR (N-H) = 2921.98 cm^{-1}; R_f (hexane/DCM:20/80) = 0.1.

Compound 5: Dry DCM (60.0 mL) which was flushed with argon for 10 minutes. The reaction flask was cooled to -78 °C and to the solution was added methyl chlorooxoacetate (0.180 mL, 1.90 mmol, 1.00 eq.) and 2,4-dimethylpyrrole (0.400 mL, 3.90 mmol, 2.50 eq.). The reaction was stirred at this temperature for four hours before TEA (1.08 mL, 7.76 mmol, 4.00 eq.) was added, followed by $BF_3{\cdot}Et_2O$ (3.00 mL, 24.0 mmol, 12.5 eq., excess). The reaction mixture was allowed to reach room temperature and stirred for a further two hours prior to the removal of solvent *in vacuo*. The crude product was purified by flash column chromatography on silica gel; eluent: hexane/DCM:50/50 and the fractions containing product were combined and concentrated by evaporation to afford methyl 5,5-difluoro-1,3,7,9-tetramethyl-5H-4λ4,5λ4-dipyrrolo[1,2-c:2',1'-f][1,3,2]diazaborinine-10-carboxylate (309 mg, 1.00 mmol, 53%) as a red solid. ^{1}H NMR (600 MHz, $CDCl_3$) δH 6.07 (s, 2H, Ar**H**), 3.97 (s, 3H, OC**H$_3$**), 2.53 (s, 6H, 2C**H$_3$**), 2.12 (s, 6H, 2C**H$_3$**) ppm; ^{13}C NMR (151 MHz, $CDCl_3$) δC 165.9, 157.8, 141.2, 128.7, 128.7, 121.3, 53.3, 14.9, 12.7 ppm; ^{11}B NMR (224 MHz, CDCl3) δB 0.55 (t, *J* = 33.3 Hz) ppm; ^{19}F NMR (658 MHz, CDCl3) δF -146.3 ppm; IR (C=O) = 1737.61 cm^{-1} ;R_f (hexane/DCM:50/50) = 0.2.

Compound 6: 2,4-dimethylpyrrole (0.500 mL, 5.00 mmol, 2.00 eq.) and oxalyl chloride (0.220 mL, 2.50 mmol, 1.00 eq.) were dissolved in dry DCM (20.0 mL) and degassed with argon. Dry ethanol (2.50 mmol, 1.00 eq.) was added and the reaction mixture was stirred at room temperature for one hour. TEA (2.00 mL) and $BF_3.Et_2O$ (3.00 mL) were added dropwise and the reaction was stirred at room temperature under argon for three hours. The solvent was subsequently removed under vacuum and the crude was purified by flash column chromatography on silica gel; eluent: hexane/DCM:50/50. Ethyl 5,5-difluoro-1,3,7,9-tetramethyl-5*H*-4λ^4,5λ^4-dipyrrolo[1,2-*c*:2',1'-*f*][1,3,2]diazaborinine-10-carboxylate (309 mg, 1.00 mmol, 53%) as an amorphous red solid. ^{1}H NMR (600 MHz, $CDCl_3$) δ_H 6.07 (s, 2H, Ar**H**), 4.43 (q, *J* = 7.2 Hz, 2H, C**H$_2$**), 2.54 (s, 6H, 2C**H$_3$**), 2.14 (s, 6H, 2C**H$_3$**), 1.43 (t, *J* = 7.2 Hz, 6H, C**H$_3$**) ppm; ^{11}B NMR (224 MHz, $CDCl_3$) δ_B 0.27 (t, *J* = 33.8 Hz) ppm; IR (C=O) = 1737.70 cm^{-1}; R_f (hexane/DCM:50/50) = 0.2.

Compound 7: 2,4-dimethylpyrrole (0.500 mL, 5.00 mmol, 2.00 eq.) and oxalyl chloride (0.220 mL, 2.50 mmol, 1.00 eq.) were dissolved in dry DCM (20.0 mL) and degassed with argon. Dry isopropyl alcohol (2.50 mmol, 1.00 eq.) was added and the reaction mixture was stirred at room temperature for one hour. TEA (2.00 mL) and $BF_3.Et_2O$ (3.00 mL) were added dropwise and the reaction was stirred at room temperature under argon for three hours. The solvent was subsequently removed under vacuum and the crude was purified by flash column chromatography on silica gel; eluent: hexane/DCM:50/50. Isopropyl 5,5-difluoro-1,3,7,9-tetramethyl-5*H*-4λ^4,5λ^4-dipyrrolo[1,2-*c*:2',1'-*f*][1,3,2]diazaborinine-10-carboxylate (322 mg, 1.00 mmol, 40%) as an amorphous red solid. ^{1}H NMR (600 MHz, $CDCl_3$) δ_H 6.08 (s, 2H, Ar**H**), 5.25 (spt, *J* = 6.3 Hz, 1H, C**H**), 2.54 (s, 6H, 2C**H$_3$**), 2.19 (s, 6H, 2C**H$_3$**), 1.43 (t, *J* = 7.2 Hz, 6H, 2C**H$_3$**) ppm; ^{11}B-NMR (224 MHz, $CDCl_3$) δ_B 0.27 (t, *J* = 33.8 Hz) ppm; IR (C=O) = 1737.68 cm^{-1}; R_f (hexane/DCM:50/50) = 0.2.

Compound 8: Acetyl chloride (0.700 mL, 9.75 mmol) and 2,4-dimethylpyrrole (2.00 mL, 19.5 mmol, 2.00 eq.) were dissolved in dry DCM (30.0 mL) under argon. The reaction mixture was heated under reflux overnight. $BF_3{\cdot}Et_2O$ (8.00 mL, 65.0 mmol, 33.0 eq.) and TEA (4.00 mL, 29.0 mmol, 15.0 eq.) were added and the reaction stirred for a further four hours. The solvent was removed under vacuum and the crude purified by flash column chromatography on silica gel; eluent: hexane/DCM(60/40). The fractions containing product were combined and concentrated in vacuo to afford 5,5-difluoro-1,3,7,9,10-pentamethyl-5H-4λ4,5λ4-dipyrrolo[1,2-c:2',1'-f][1,3,2]diazaborinine (1.06 g, 4.04 mmol, 41%). ^{1}H NMR (700 MHz, $CDCl_3$) δH 6.05 (s, 2H, Ar**H**), 2.58 (s, 3H, C**H$_3$**), 2.52 (s, 6H, 2C**H$_3$**), 2.42 (s, 6H, 2C**H$_3$**) ppm; ^{11}B NMR (224 MHz, $CDCl_3$) δB 0.62 (t, *J* = 33.3 Hz) ppm; ^{19}F NMR (658 MHz, CDCl3) δF -146.7 (q, *J* = 33.1 Hz) ppm; Rf (hexane/DCM:70/30) = 0.1.

Compounds 9 and 10: 2,4-dimethylpyrrole (0.12 mL, 1.2 mmol, 2 eq.) and glutaric or succinic anhydride (0.6 mmol, 1 eq.) were dissolved in dry DCM (10 mL) under argon. $BF_3{\cdot}Et_2O$ (0.5 mL, 4 mmol) and TEA (0.42 mL, 3 mmol) were added and the reaction heated under reflux for five hours. The organic material was washed with water, dried over $MgSO_4$, filtered and concentrated *in vacuo* before purification by flash column chromatography on silica gel; eluent: hexane/EtOAc/AcOH:50/50/0 to 0/97/3**. Compound 9**: 4-(5,5-difluoro-1,3,7,9-tetramethyl-5H-4l4,5l4-dipyrrolo[1,2-c:2',1'-f][1,3,2]diazaborinin-10-yl)butanoic acid (22.0 mg, 0.066 mmol, 11%). ^{1}H NMR (600.130 MHz, $CDCl_3$) δ_H 6.06 (s, 2H, Ar**H**), 2.82-2.78 (m, 2H, C**H$_2$**), 2.57-2.54 (m, 2H, C**H$_2$**), 2.52 (s, 6H, 2C**H$_3$**), 2.43 (s, 6H, 2C**H$_3$**), 2.04-1.99 (m, 2H, C**H$_2$**) ppm; IR (C=O) = 1687.50 cm^{-1}, (O-H) = 3266.48 cm^{-1}; R_f (EtOAc) = 0.3 (stained with bromocresol green). **Compound 10**: 3-(5,5-difluoro-1,3,7,9-tetramethyl-5H-4l4,5l4-dipyrrolo[1,2-c:2',1'-f][1,3,2]diazaborinin-10-yl)propanoic acid (27.0 mg, 0.084 mmol, 14%).^{1}H

NMR (600.130 MHz, $CDCl_3$) δ_H 6.06 (s, 2H, Ar**H**), 3.36-3.33 (m, 2H, C**H$_2$**), 2.71-2.69 (m, 2H, C**H$_2$**), 2.52 (s, 6H, 2C**H$_3$**), 2.45 (s, 6H, 2C**H$_3$**) ppm; IR (C=O) = 1688.71 cm^{-1}, (O-H) = 3266.60 cm^{-1}; R_f (EtOAc) = 0.3 (stained with bromocresol green).

Compounds 11 and 12: Compound **1** or **5** were dissolved in dry THF (10 mL) under argon and cooled to -78 °C. NIS (3.9 eq.) was added and the reaction warmed to room temperature overnight. The solvent was evaporated and the crude purified by flash column chromatography on silica gel; eluent: hexane/DCM:50/50. **Compound 11**: (5,5-difluoro-2,8-diiodo-1,3,7,9-tetramethyl-5*H*-4λ^4,5λ^4-dipyrrolo[1,2-*c*:2',1'-*f*][1,3,2]diazaborinin-10-yl)methyl acetate (61.0 mg, 0.109 mmol, 33%) ^{1}H NMR (600.130 MHz, $CDCl_3$) δ_H 4.01(s, 3H, OC**H$_3$**), 2.64 (s, 6H, 2C**H$_3$**), 2.14 (s, 6H, 2C**H$_3$**) ppm; ^{11}B-NMR (224 MHz, $CDCl_3$) δ_B 0.38 (t, *J* = 30.5 Hz) ppm; ^{19}F-NMR (658 MHz, $CDCl_3$) δ_F -145.7 (q, *J* = 31.6 Hz) ppm; IR (C=O) = 1737.11 cm^{-1}; R_f (hexane/DCM:50/50) = 0.2. **Compound 12**: methyl 5,5-difluoro-2,8-diiodo-1,3,7,9-tetramethyl-5*H*-4λ^4,5λ^4-dipyrrolo[1,2-*c*:2',1'-*f*][1,3,2]diazaborinine-10-carboxylate (52.0 mg, 0.091 mmol, 29%) ^{1}H NMR (600.130 MHz, $CDCl_3$) δ_H 5.32 (s, 2H, C**H$_2$**), 2.63 (s, 6H, 2C**H$_3$**), 2.40 (s, 6H, 2C**H$_3$**), 2.15 (s, 3H C**H$_3$**) ppm; ^{13}C NMR (151 MHz, $CDCl_3$) δ_C 170.4, 158.1, 143.6, 132.9, 132.7, 87.4, 58.4, 20.7, 18.3, 16.5 ppm; ^{11}B-NMR (224 MHz, $CDCl_3$) δ_B 0.36 (t, *J* = 33.3 Hz) ppm; ^{19}F-NMR (658 MHz, $CDCl_3$) δ_F -145.6 (q, *J* = 31.6 Hz) ppm; IR (C=O) = 1740.76 cm^{-1}; R_f (hexane/DCM:50/50) = 0.4.

Compound 13: A solution of (5,5-difluoro-1,3,7,9-tetramethyl-5*H*-4λ^4,5λ^4-dipyrrolo[1,2-*c*:2',1'-*f*][1,3,2] diazaborinin-10-yl)methyl acetate (100 mg, 0.310 mmol) was prepared in dry toluene (300 mL). Methyl 4-ethynyl benzoate (124 mg, 0.775 mmol, 2.50 eq.), Pd(tetrakis) (10.4 mg, 0.00900 mmol, 3.00 mol%), CuI (3.00 mg, 0.0160 mmol, 5.00 mol%) and TEA (3.00 mL) were added and the reaction mixture stirred under reflux overnight. The reaction mixture was filtered through a plug of celite using EtOAc and the crude product dried under vacuum. The material was purified using flash column chromatography on silica gel; eluent: hexane/EtOAc:10/90. The fractions containing product were combined and concentrated *in vacuo* to afford 4,4'-((5,5-difluoro-1,3,7,9,10-pentamethyl-5*H*-4λ^4,5λ^4-dipyrrolo[1,2-c:2',1'-f][1,3,2]diazaborinine-2,8-diyl)bis(ethyne-2,1-diyl))dibenzoate as an amorphous purple solid (27.0 mg, 0.0467 mmol, 15%). ^{1}H-NMR (700 MHz, $CDCl_3$) δ_H 8.03 (d, 4H, *J* = 8.5 Hz, Ph**H**), 7.57 (d, 4H, *J* = 8.5 Hz, Ph**H**), 3.94 (s, 6H, COOC**H$_3$**), 2.71 (s, 3H, C**H$_3$**), 2.70 (s, 6H, 2C**H$_3$**), 2.60 (s, 6H, 2C**H$_3$**) ppm; ^{11}B-NMR (224 MHz, $CDCl_3$) δ_B 0.59 (t, *J* = 30.5 Hz) ppm; ^{19}F-NMR (658 MHz, $CDCl_3$) δ_F -146.6 (q, *J* = 31.6 Hz) ppm; IR (C=O) = 1719.33 cm^{-1}; R_f (hexane/EtOAc:20/80) = 0.1.

Compound 14: A solution of (5,5-difluoro-1,3,7,9-tetramethyl-5*H*-4λ^4,5λ^4-dipyrrolo[1,2-*c*:2',1'-*f*][1,3,2] diazaborinin-10-yl)methyl acetate (100 mg, 0.310 mmol) was prepared in dry toluene (30 mL). 4-ethynyl-*N,N*-dimethylaniline (113 mg, 0.775 mmol, 2.50 eq.), Pd(tetrakis) (10.4 mg, 0.009 mmol, 3.0 mol%), CuI (3.00 mg, 0.0160 mmol, 5.00 mol%) and TEA (3.00 mL) were added and the reaction mixture stirred under reflux overnight. The reaction mixture was filtered through a plug of celite using EtOAc and the crude product dried under vacuum. The material was purified using flash column chromatography on silica gel; eluent: hexane/EtOAc:50/50. The fractions containing product were combined and concentrated by evaporation to yield 4,4'-((5,5-difluoro-1,3,7,9,10-pentamethyl-5*H*-4λ^4,5λ^4-dipyrrolo[1,2-c:2',1'-f][1,3,2]diazaborinine-2,8-diyl)bis(ethyne-2,1-diyl))bis(N,N-dimethylaniline) as an amorphous purple solid (21.0 mg, 0.0383 mmol, 12%). ^{1}H NMR (700 MHz, $CDCl_3$) δ_H 7.40 (d, 4H, *J* = 8.9 Hz, Ph**H**), 6.67 (d, 4H, *J* = 8.7 Hz, Ph**H**), 3.00 (s, 12H, 2N(C**H$_3$**)$_2$), 2.68 (s, 6H, 2C**H$_3$**), 2.67 (s, 3H, C**H$_3$**), 2.56 (s, 6H, 2C**H$_3$**) ppm; ^{11}B NMR (224 MHz, $CDCl_3$) δ_B 0.46 (t, *J* = 33.3 Hz) ppm; ^{19}F NMR (658 MHz, $CDCl_3$) δ_F – 146.9 (q, *J* = 31.9 Hz) ppm; R_f (hexane/EtOAc:50/50) = 0.2.

Compound 15: An oven dried round bottomed flask was equipped with a Dean-Stark trap and charged with benzaldehyde (0.110 mL, 1.10 mmol, 2.20 eq.), piperidine (2.00 mL) and AcOH (2.00 mL). The flask was flushed with argon before methyl 5,5-difluoro-1,3,7,9-tetramethyl-5*H*-4λ^4,5λ^4-dipyrrolo[1,2-*c*:2',1'-*f*][1,3,2]diazaborinine-10-carboxylate (150 mg, 0.490 mmol, 1.00 eq.) in dry toluene (20.0 mL) was added. The flask was equipped with a Dean and Stark trap and the reaction mixture was heated under reflux for 16 hours. After cooling to room temperature, the reaction mixture was washed with distilled water (3 x 20.0 mL) and the organic material was extracted with DCM, dried over $MgSO_4$, filtered and concentrated *in vacuo*. The residue was purified by flash column chromatography on silica gel; eluent: DCM/MeOH from a ratio of 100/0 to 90/10. The fractions containing product were combined and concentrated by evaporation to afford methyl 5,5-difluoro-1,9-dimethyl-3,7-di((E)-styryl)-5H-4λ^4,5λ^4-dipyrrolo[1,2-c:2',1'-f][1,3,2]diazaborinine-10-carboxylate as a blue solid (140 mg, 0.290 mmol, 59%). ^{1}H-NMR (700 MHz, $CDCl_3$) δ_H 7.70 (d, *J* = 16.4 Hz, 2H, C=C**H**), 7.53 (d, *J* = 16.3 Hz, 4H, Ph**H**), 7.42 (m, 6H, Ph**H**), 7.10 (d, *J* = 16.4 Hz, 2H, C=C**H**), 6.72 (s, 2H, Ar**H**), 4.01 (s, 3H, C**H$_3$**), 2.20 (s, 6H, 2C**H$_3$**) ppm; ^{11}B-NMR (224 MHz, $CDCl_3$) δ_B 0.98 (t, *J* = 33.3 Hz) ppm; ^{19}F-NMR (658 MHz, $CDCl_3$) δ_F -138.3 ppm; MS (ESI) $C_{29}H_{25}BF_2N_2O_2$ (*m/z* 483.2, [M+H]$^+$; IR (C=O) = 1735.80 cm^{-1}; R_f (DCM) = 0.2.

Compound 16: Dry toluene (30.0 mL) was degassed with argon for 30 minutes. 10-(bromomethyl)-5,5-difluoro-1,3,7,9-tetramethyl-5*H*-4λ^4,5λ^4-dipyrrolo[1,2-*c*:2',1'-*f*][1,3,2]diazaborinine (80.0 mg, 0.235 mmol) was added followed by diethylaminobenzaldehyde (92.0 mg, 0.517 mmol, 2.2 eq.). AcOH (2.00 mL) and piperidine (2.00 mL) were added and the reaction mixture was stirred under reflux and under argon overnight. The organic material was extracted using DCM and the organic layers washed with water, dried over $MgSO_4$, filtered and concentrated by evaporation. The crude solid was purified by flash column chromatography on silica gel; eluent: hexane/DCM. The fractions containing product were combined and concentrated under vacuum to afford 4,4'-((1*E*,1'*E*)-(10-(bromomethyl)-5,5-difluoro-1,9-dimethyl-5*H*-4λ^4,5λ^4-dipyrrolo[1,2-c:2',1'-f][1,3,2]diazaborinine-3,7-diyl)bis(ethene-2,1-diyl))bis(*N,N*-diethylaniline) as a green/blue solid (10.0 mg, 0.0160 mmol, 7%). ^{1}H-NMR (700 MHz, $CDCl_3$) δ_H 7.47 (d, *J* = 8.8 Hz, 4H, Ar**H**), 7.45 (d, *J* = 16.7 Hz, 2H, C=C**H**), 7.20 (d, *J* = 16.1 Hz, 2H, C=C**H**), 6.67 (s, 2H, C**H**), 6.64 (d, *J* = 8.8 Hz, 4H, Ar**H**) 3.72 (s, 2H C**H$_2$**Br), 3.40 (q, *J* = 7.1 Hz, 8H, C**H$_2$**CH$_3$), 2.51 (s, 6H, C**H$_3$**), 1.19 (t, *J* = 7.1 Hz, 12H, CH$_2$C**H$_3$**) ppm; ^{11}B-NMR (224 MHz, $CDCl_3$) δ_B 0.86 (t, *J* = 33.3 Hz) ppm; ^{19}F-NMR (658 MHz, $CDCl_3$) δ_F -142.5 ppm; R_f (hexane/EtOAc:60/40) = 0.3.

HiBO: Dry DCM (150 mL) was purged with argon for 30 min. Bromoacetyl bromide (0.170 mL, 1.90 mmol, 1 eq.) and 2,4-dimethylpyrrole (0.400 mL, 3.90 mmol, 2 eq.) were added dropwise and the dark red reaction mixture was stirred at room temperature under argon and protected from the light for three hours. The solvent was reduced to ~50 mL under vacuum and triethylamine (4.00 mL, 29.0 mmol, 15 eq.) was added. After 15 min of stirring under argon, $BF_3{\cdot}Et_2O$ (8.00 mL, 65.0 mmol, 33 eq.) was added dropwise. The reaction mixture was stirred for a further three hours under argon and protected from the light. DCM (3 x 30 mL) was used to extract the organic material which was washed with distilled water (3 x 30 mL), dried over $MgSO_4$, filtered and concentrated *in vacuo*. The crude red product was purified by flash column chromatography on silica gel; eluent: hexane/DCM from a ratio of 80/20 to 50/50. The fractions containing product were combined and concentrated by evaporation to afford 10-(bromomethyl)-5,5-difluoro-1,3,7,9-tetramethyl-5*H*-4λ^4,5λ^4-dipyrrolo[1,2-*c*:2',1'-*f*][1,3,2]diazaborinine (224 mg, 0.660 mmol, 35%) as a red solid. ^{1}H-NMR (600 MHz, $CDCl_3$) δ_H 6.09 (s, 2H, C**H**), 4.69 (s, 2H, C**H$_2$**Br), 2.54 (s, 12H, 4C**H$_3$**) ppm; ^{13}C-NMR (151 MHz, $CDCl_3$) δ_C 156.6, 141.0, 137.3, 131.1, 122.4, 24.7, 16.1, 14.8 ppm; MS (EI) $C_{14}H_{16}BBrF_2N_2$ (*m/z* 340.1,

[M{^{79}Br}+H]$^+$; *m/z* 342.1, [M{^{81}Br}+H]$^+$; *m/z* 261.1, [M-Br+H]$^+$), R_f (hexane/EtOAc:60/40) = 0.3.

Acknowledgements

The authors would like to thank Dr. Abil Aliev, Dr. Edoardo Scarpa, and Dr. Jonathan R. Burns, at UCL Chemistry for assisting in NMR analysis, providing cells, and helping with the creation of figures, respectively. The authors also want to thank Conor Lanphere and Helena Philpott for critically reading the manuscript and providing valuable feedback. J.W. is supported by the Leverhulme Trust (RPG-2019-183). S.H. is supported by the Leverhulme Trust (RPG-2017-015) and B. P is supported by the EPSRC (EP/N026322/1) and ERC (769798). T.M.C. would like to acknowledge support from EPSRC project EP/N026411/1.

Keywords: Fluorophores • near-infrared • lipid bilayer • confocal fluorescence microscopy • BODIPY

1 D. Gatica, V. Lahiri and D. J. Klionsky, *Nat. Cell Biol.*, 2018, **20**, 233–242.

2 M. Fernández-Suárez and A. Y. Ting, *Nat. Rev. Mol. Cell Biol.*, 2008, **9**, 929–943.

3 J.-S. Lee, N. Kang, Y. K. Kim, A. Samanta, S. Feng, H. K. Kim, M. Vendrell, J. H. Park and Y.-T. Chang, *J. Am. Chem. Soc.*, 2009, **131**, 10077–10082.

4 S. H. Alamudi, R. Satapathy, J. Kim, D. Su, H. Ren, R. Das, L. Hu, E. Alvarado-Martínez, J. Y. Lee, C. Hoppmann, E. Peña-Cabrera, H.-H. Ha, H.-S. Park, L. Wang and Y.-T. Chang, *Nat. Commun.*, 2016, **7**, 11964.

5 A. Loudet and K. Burgess, *Chem. Rev.*, 2007, **107**, 4891–4932.

6 D. Wu and D. F. O'Shea, *Chem. Commun.*, 2017, **53**, 10804–10807.

7 O. S. Vodyanova, B. A. Kochergin, S. D. Usoltsev, Y. S. Marfin, E. V. Rumyantsev, E. L. Aleksakhina and I. K. Tomilova, *J. Photochem. Photobiol. A Chem.*, 2018, **350**, 44–51.

8 T. Gayathri, A. K. Barui, S. Prashanthi, C. R. Patra and S. P. Singh, *RSC Adv.*, 2014, **4**, 47409–47413.

9 J. H. Gibbs, Z. Zehua, D. Kessel, F. R. Fronczek, S. Pakhomova and M. G. H. Vicente, *J. Photochem. Photobiol. B Biol.*, 2015, **145**, 35–47.

10 M. Bacalum, L. Wang, S. Boodts, P. Yuan, V. Leen, N. Smisdom, E. Fron, S. Knippenberg, G. Fabre, P. Trouillas, D. Beljonne, W. Dehaen, N. Boens and M. Ameloot, *Langmuir*, 2016, **32**, 3495–3505.

11 Y. Ni, L. Zeng, N. Y. Kang, K. W. Huang, L. Wang, Z. Zeng, Y. T. Chang and J. Wu, *Chem. - A Eur. J.*, 2014, **20**, 2301–2310.

12 B. W. Michel, A. R. Lippert and C. J. Chang, *J. Am. Chem. Soc.*, 2012, **134**, 15668–15671.

13 G. Ulrich, R. Ziessel and A. Harriman, *Angew. Chemie - Int. Ed.*, 2008, **47**, 1184–1201.

14 K. Umezawa, Y. Nakamura, H. Makino, D. Citterio and K. Suzuki, *J. Am. Chem. Soc.*, 2008, **130**, 1550–1551.

15 T. Slanina, P. Shrestha, E. Palao, D. Kand, J. A. Peterson, A. S. Dutton, N. Rubinstein, R. Weinstain, A. H. Winter and P. Klán, *J. Am. Chem. Soc.*, 2017, **139**, 15168–15175.

16 A. Treibs and F.-H. Kreuzer, *Justus Liebigs Ann. Chem.*, 1968, **718**, 208–223.

17 L. Mendive-Tapia, C. Zhao, A. R. Akram, S. Preciado, F. Albericio, M. Lee, A. Serrels, N. Kielland, N. D. Read, R. Lavilla and M. Vendrell, *Nat. Commun.*, 2016, **7**, 10940.

18 R. Subiros-Funosas, L. Mendive-Tapia, J. Sot, J. D. Pound, N. Barth, Y. Varela, F. M. Goñi, M. Paterson, C. D. Gregory, F. Albericio, I. Dransfield, R. Lavilla and M. Vendrell, *Chem. Commun.*, 2017, **53**, 945–948.

19 A. Vázquez-Romero, N. Kielland, M. J. Arévalo, S. Preciado, R. J. Mellanby, Y. Feng, R. Lavilla and M. Vendrell, *J. Am. Chem. Soc.*, 2013, **135**, 16018–16021.

20 S. Kolemen, Y. Cakmak, S. Erten-Ela, Y. Altay, J. Brendel, M. Thelakkat and E. U. Akkaya, *Org. Lett.*, 2010, **12**, 3812–3815.

21 H. Sunahara, Y. Urano, H. Kojima and T. Nagano, *J. Am. Chem. Soc.*, 2007, **129**, 5597–5604.

22 T. Rohand, W. Qin, N. Boens and W. Dehaen, *European J. Org. Chem.*, 2006, **2006**, 4658–4663.

23 L. Fournier, I. Aujard, T. Le Saux, S. Maurin, S. Beaupierre, J. B. Baudin and L. Jullien, *Chem. - A Eur. J.*, 2013, **19**, 17494–17507.

24 S. Yin, V. Leen, S. Van Snick, N. Boens and W. Dehaen, *Chem. Commun.*, 2010, **46**, 6329.

25 J. C. Er, M. K. Tang, C. G. Chia, H. Liew, M. Vendrell and Y.-T. Chang, *Chem. Sci.*, 2013, **4**, 2168.

26 S. Kusaka, R. Sakamoto, Y. Kitagawa, M. Okumura and H. Nishihara, *Chem. - An Asian J.*, 2013, **8**, 723–727.

27 X.-F. Zhang and N. Feng, *Chem. - An Asian J.*, 2017, **12**, 2447–2456.

28 H. P. Nguyen, S. Stewart, M. N. Kukwikila, S. F. Jones, D. Offenbartl-Stiegert, S. Mao, S. Balasubramanian, S. Beck and S. Howorka, *Angew. Chemie - Int. Ed.*, 2019, **58**, 6620–6624.

29 D. Offenbartl-Stiegert, T. M. Clarke, H. Bronstein, H. P. Nguyen and S. Howorka, *Org. Biomol. Chem.*, 2019, **17**, 6178–6183.

30 S. Sahu, A. Sharma and A. K. Mishra, *J. Phys. Chem. B*, 2018, **122**, 7308–7318.

10.1002/chem.201904164

31 E. C. Jensen, *Anat. Rec. Adv. Integr. Anat. Evol. Biol.*, 2012, **295**, 2031–2036.

32 B. Guo, X. Cai, S. Xu, S. M. A. Fateminia, J. Liu, J. Liang, G. Feng, W. Wu and B. Liu, *J. Mater. Chem. B*, 2016, **4**, 4690–4695.

33 M. J. Garland, C. M. Cassidy, D. Woolfson and R. F. Donnelly, *Future Med. Chem.*, 2009, **1**, 667–691.

34 S. Sri, R. Kumar, A. K. Panda and P. R. Solanki, *ACS Appl. Mater. Interfaces*, 2018, **10**, 37835–37845.

35 P. Chidchob, D. Offenbartl-Stiegert, D. McCarthy, X. Luo, J. Li, S. Howorka and H. F. Sleiman, *J. Am. Chem. Soc.*, 2019, **141**, 1100–1108.

36 R. Xie, Y. Yi, Y. He, X. Liu and Z.-X. Liu, *Tetrahedron*, 2013, **69**, 8541–8546.

10.1002/chem.201904164

WILEY-VCH

Entry for the Table of Contents

FULL PAPER

Designer fluorophores: a library of BODIPY analogues with systematic variation at defined points around the molecule's core was used to create a correlation table predicting accurately the properties of a designer membrane dye which has the ability to stain cells.

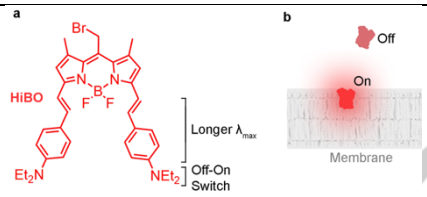

Joanna L. Donnelly, Daniel Offenbartl-Stiegert, Loris Rizello, Guiseppe Battaglia, Stefan Howorka, and Jonathan D. Wilden**

Page No. – Page No.

Preparation, Evaluation and Application of BODIPY Dyes: Designer Fluorophores for Targeted Biological Applications

J. L. Donnelly, Daniel Offenbartl-Stiegert, Dr. L. R
Battaglia, Prof. S. Howorka and Dr. J. D. Wilden
Department of Chemistry, University College Lon
20 Gordon Street, London, WC1H 0AJ (UK)
E-mail: j.wilden@ucl.ac.uk; s.howorka@ucl.ac.uk

J. L. Donnelly, Daniel Offenbartl-Stiegert, Prof. S.
J. D. Wilden, Institute of Structural and Molecular
College London
20 Gordon Street, London, WC1H 0AJ (UK)

L. Rizzello and Prof. G. Battaglia
Institute of Physics of Living System, University C
Gower Street, London, WC1E 6BT

L. Rizzello and Prof. G. Battaglia
IBEC-Institute for Bioengineering of Catalonia, Th